Near-Far Description of Elastic and Breakup Reactions of Halo Nuclei

Mahir Hussein[1]

Instituto de Física, Universidade de São Paulo C.P. 66318, 05315-970 São Paulo, S.P., Brazil

E-mail: hussein@if.usp.br

Pierre Capel, Daniel Baye

Physique Nucléaire et Physique Quantique (CP 229), Université Libre de Bruxelles, B-1050 Brussels, Belgium

E-mail: pierre.capel@ulb.ac.be, dbaye@ulb.ac.be

Abstract. The angular distributions for elastic scattering and breakup of halo nuclei are analysed using a near-side/far-side decomposition within the framework of the dynamical eikonal approximation. This analysis is performed for ^{11}Be impinging on Pb at 69AMeV. These distributions exhibit very similar features. In particular they are both near-side dominated, as expected from Coulomb-dominated reactions. The general shape of these distributions is sensitive mostly to the projectile-target interactions, but is also affected by the extension of the halo. This suggests that the link between elastic scattering and a possible loss of flux towards the breakup channel is not obvious.

1. Introduction

The development of radioactive-ion beams in the mid-80s has enabled the exploration of the nuclear landscape away from stability. This technical breakthrough led to the discovery of exotic nuclear structures such as halœs [1, 2]. Halo nuclei are light neutron-rich nuclei, which exhibit a matter radius significantly larger than their isobars. This large size is qualitatively understood as resulting from their small binding energy for one or two neutrons [3]: Due to their loose binding, these valence neutrons can tunnel far away from the core of the nucleus and exhibit a large probability of presence at a large distance from the other nucleons. Halo nuclei have thus a strongly clusterised structure: they can be seen as a core to which one or two neutrons are loosely bound. These valence neutrons hence form a sort of diffuse halo around a compact core. The best known halo nuclei are ^{11}Be and ^{15}C, with a one-neutron halo, and ^{6}He and ^{11}Li, with a two-neutron halo. Proton halœs can also develop around proton-rich nuclei, such as ^{8}B or ^{17}F.

Since their discovery, halo nuclei have been at the centre of many studies, both experimental [4, 5] and theoretical [6, 7]. Due to their short lifetime, they cannot be studied with usual spectroscopic techniques, and one must resort to indirect methods to deduce information about their structure. Reactions are the most used tools to study halo nuclei. In particular, elastic

[1] Speaker

scattering [8, 9] and breakup [10, 11] convey interesting information about the structure of the projectile.

Recent experimental [9] and theoretical [8] studies of elastic scattering indicate a strong coupling between scattering and breakup. On the experimental side, the elastic scattering cross section for ^{11}Be on Zn around the Coulomb barrier is significantly reduced at large angles compared to that of non-halo Be isotopes [9]. One explanation of this unexpected reduction is the transfer of probability flux from the elastic channel to the breakup channel. On the theoretical side, Matsumoto *et al* have shown that for the elastic scattering of ^{6}He on Bi at low energy CDCC calculations agree with experimental data only if the breakup channel is included in the model space.

To better investigate the interplay between elastic scattering and breakup, we analyse theoretically the angular distributions for the elastic scattering and breakup of halo nuclei within a near/far decomposition [12, 13]. We choose ^{11}Be, the archetypical one-neutron halo nucleus, as testcase and consider its collision on Pb at 69AMeV, which corresponds to the conditions of the RIKEN experiment [10]. The calculations are performed within the Dynamical Eikonal Approximation (DEA) [11, 14], which is in excellent agreement with various experimental results.

After a brief reminder of the DEA and the near/far decomposition, we apply this technique to the elastic-scattering cross section (Sec. 3). We then move to the analysis of the angular distribution for breakup (Sec. 4) and show how similar both cross sections are at intermediate energies. In Sec. 5, we emphasise the consequences of this analysis for the study of halo nuclei and provide the prospects of this work.

2. Theoretical framework

2.1. Dynamical eikonal approximation

Most of the models of reactions involving one-neutron halo nuclei rely on a three-body description of the colliding nuclei [6, 15]: a two-body projectile P made up of a fragment f loosely bound to a core c impinging on a structureless target T. The two-body structure of the projectile is described by the phenomenological Hamiltonian

$$H_0 = -\frac{\hbar^2}{2\mu_{cf}}\Delta_{\boldsymbol{r}} + V_{cf}(\boldsymbol{r}), \tag{1}$$

where $\boldsymbol{r}$ is the c-f relative coordinate, μ_{cf} is the c-f reduced mass, and V_{cf} is a real potential adjusted to reproduce the binding energy of the fragment to the core and some of the excited states of the projectile. This potential usually exhibits a Woods-Saxon form factor and may include a spin-orbit coupling term.

The interaction between the projectile components c and f and the target T are simulated by the optical potentials V_{cT} and V_{fT}, respectively. Within this three-body framework, studying reactions involving one-neutron halo nuclei reduces to solve the three-body Schrödinger equation

$$\left[-\frac{\hbar^2}{2\mu}\Delta_{\boldsymbol{R}} + H_0 + V_{cT}(\boldsymbol{r},\boldsymbol{R}) + V_{fT}(\boldsymbol{r},\boldsymbol{R})\right]\Psi(\boldsymbol{r},\boldsymbol{R}) = E_{\rm tot}\Psi(\boldsymbol{r},\boldsymbol{R}), \tag{2}$$

where $\boldsymbol{R}$ is the P-T relative coordinate, μ is the P-T reduced mass and

$$E_{\rm tot} = E_0 + \frac{\hbar^2 K^2}{2\mu} \tag{3}$$

is the total energy of the system, with E_0 the (negative) energy of the projectile ground state $\phi_{l_0 j_0 m_0}$ and $\hbar K$ the initial P-T relative momentum. The quantum numbers l_0, j_0 and m_0

correspond to the c-f orbital angular momentum, the projectile total angular momentum and its projection, respectively.

To describe a reaction in which the halo nucleus P impinges on the target T, Eq. (2) is solved with the initial condition

$$\Psi^{(m_0)}(\boldsymbol{r},\boldsymbol{b},Z) \underset{Z\to-\infty}{\longrightarrow} e^{iKZ}\phi_{l_0j_0m_0}, \tag{4}$$

where the dependence upon the transverse $\boldsymbol{b}$ and longitudinal Z components of $\boldsymbol{R}$ is made explicit. Equation (2) must be solved for each value of $\boldsymbol{b}$ and of m_0.

At sufficiently high incident energy, the eikonal approximation can be performed to ease the resolution of Eq. (2). That approximation consists in assuming that most of the rapid variation of Ψ in the P-T relative coordinate $\boldsymbol{R}$ is included in the plane wave e^{iKZ}, i.e. that the three-body wave function is well approximated by that plane wave times a function $\widehat{\Psi}$ that does not vary much with $\boldsymbol{R}$:

$$\Psi(\boldsymbol{r},\boldsymbol{b},Z) = e^{iKZ}\widehat{\Psi}(\boldsymbol{r},\boldsymbol{b},Z). \tag{5}$$

Including the eikonal ansatz (5) within Eq. (2) leads to

$$\left[-\frac{\hbar^2}{2\mu}\Delta_{\boldsymbol{R}} - i\frac{\hbar^2K}{\mu}\frac{\partial}{\partial Z} + \frac{\hbar^2K^2}{2\mu} + H_0 + V_{cT}(\boldsymbol{r},\boldsymbol{R}) + V_{fT}(\boldsymbol{r},\boldsymbol{R})\right]\widehat{\Psi}(\boldsymbol{r},\boldsymbol{R}) = E_{\rm tot}\widehat{\Psi}(\boldsymbol{r},\boldsymbol{R}). \tag{6}$$

Since $\widehat{\Psi}$ varies smoothly with $\boldsymbol{R}$, its second-order derivative $\Delta_{\boldsymbol{R}}\widehat{\Psi}$ can be neglected in front of its first-oder derivative $K\partial/\partial Z\widehat{\Psi}$. Then, considering the energy conservation (3), the three-body Schrödinger equation (6) reduces to the DEA equation [11, 14]

$$i\hbar v\frac{\partial}{\partial Z}\widehat{\Psi}(\boldsymbol{r},\boldsymbol{R}) = \left[H_0 - E_0 + V_{cT}(\boldsymbol{r},\boldsymbol{R}) + V_{fT}(\boldsymbol{r},\boldsymbol{R})\right]\widehat{\Psi}(\boldsymbol{r},\boldsymbol{R}), \tag{7}$$

with $v = \hbar K/\mu$ the initial P-T relative velocity. This equation is mathematically equivalent to a time-dependent Schrödinger equation with straight-line trajectories posing $Z = vt$. It can thus been solved using appropriate algorithms, such as the one described in Ref. [16]. However, since the DEA does not assume any semiclassical treatment of the P-T relative motion, $\boldsymbol{b}$ and Z are quantal variables. This implies that the DEA includes quantal interferences such as between different trajectories, which are missing in time-dependent models [14]. The DEA therefore significantly improves these models.

The DEA differs also from what is usually called the eikonal approximation [15]. In its usual form, the eikonal approximation includes a subsequent adiabatic approximation to Eq. (7) in which the excitation energy of the projectile is neglected, i.e. $H_0 - E_0 \approx 0$. In that case, the solution of Eq. (7) is approximated by the eikonal form factor

$$\widehat{\Psi}^{(m_0)}_{\rm eik}(\boldsymbol{r},\boldsymbol{b},Z\to\infty) = e^{i\chi(\boldsymbol{r},\boldsymbol{b})}\phi_{l_0j_0m_0}(\boldsymbol{r}), \tag{8}$$

where the eikonal phase reads

$$\chi(\boldsymbol{r},\boldsymbol{b}) = -\frac{1}{\hbar v}\int_{-\infty}^{\infty}[V_{cT}(\boldsymbol{r},\boldsymbol{b},Z) + V_{fT}(\boldsymbol{r},\boldsymbol{b},Z)]dZ. \tag{9}$$

The DEA thus improves the usual eikonal approximation by including dynamical effects that are otherwise neglected. These effects may be very significant such as in Coulomb breakup, for which the usual eikonal approximation diverges [14].

The DEA has been used successfully to describe elastic scattering and breakup of one-neutron halo nuclei on both light and heavy targets [14]. This approximation has also provided a reliable description of the Coulomb breakup of the one-proton halo nucleus ^{8}B [17]. More recently, a comparison of various reaction models has shown that the DEA is in excellent agreement with CDCC at intermediate energies [18] while being much less demanding on a computational point of view. The DEA is thus the most efficient model to study reactions involving one-neutron halo nuclei at intermediate energies. Moreover as it describes simultaneously both elastic scattering and breakup, the DEA is ideal for the present study.

2.2. Angular distributions and their near/far decompositions

Within the DEA, the angular distribution for elastic scattering, i.e. the elastic-scattering cross section, reads [14]

$$\frac{d\sigma_{\rm el}}{d\Omega} = K^2 \frac{1}{2j_0+1} \sum_{m_0 m_0'} \left| \int_0^\infty b db J_{|m_0'-m_0|}(qb) S_{m_0'}^{(m_0)}(b) \right|^2, \tag{10}$$

where J_μ is a Bessel function [19], $q = 2K\sin\theta/2$ is the transferred momentum and

$$S_{m_0'}^{(m_0)}(\boldsymbol{b}) = \langle \phi_{l_0 j_0 m_0'} | \widehat{\Psi}^{(m_0)}(\boldsymbol{b}, Z\to\infty) \rangle - \delta_{m_0' m_0}. \tag{11}$$

To have a better insight into the reaction mechanism that takes place during the scattering of the projectile by the target, we perform a near/far decomposition of the elastic-scattering cross section (10) [12, 13]. The idea behind this decomposition is to express the Bessel function as the sum of two Hankel functions [19]:

$$J_\mu(z) = \frac{1}{2}\left[H_\mu^{(1)}(z) + H_\mu^{(2)}(z)\right]. \tag{12}$$

The elastic-scattering cross section can then be expressed as the sum of two terms obtained by substituting J_μ by either $H_\mu^{(1)}/2$ or $H_\mu^{(2)}/2$ in Eq. (10). The former is called the *Far side* (F) of the angular distribution (10), while the latter is its *Near side* (N):

$$\frac{d\sigma_{\rm el}^{\rm F,N}}{d\Omega} = K^2 \frac{1}{2j_0+1} \sum_{m_0 m_0'} \left| \int_0^\infty b db H_{|m_0'-m_0|}^{(1,2)}(qb) S_{m_0'}^{(m_0)}(b) \right|^2. \tag{13}$$

Since these two terms add coherently to form the elastic-scattering cross section, they may interfere when they reach similar magnitude, which explains some of the oscillatory patterns observed in angular distributions [13].

The physics behind this decomposition can be understood from the asymptotic behaviour of the Hankel functions:

$$H_\mu^{(1,2)} \underset{z\to\infty}{\longrightarrow} \sqrt{\frac{2}{\pi z}} e^{\pm i(z-\mu\pi/2-\pi/4)}. \tag{14}$$

Since $q \approx K\theta$, the N side corresponds to the positive deflection i.e. repulsive forces (see Fig. 1). On the contrary the F side carries information about negative deflection, i.e. attractive forces.

The angular distribution for the breakup of the projectile can also be computed within the DEA [14]. It corresponds to the breakup cross section expressed as a function of the scattering angle $\Omega \equiv (\theta, \varphi)$ of the c-f centre of mass after dissociation at a c-f relative energy $E = \hbar^2 k^2 / 2\mu_{cf}$. It reads

$$\frac{d\sigma_{\rm bu}}{dE d\Omega} = \frac{2\mu_{cf} K K'}{\pi\hbar^2 k} \frac{1}{2j_0+1} \sum_{m_0} \sum_{ljm} \left| \int_0^\infty b db J_{|m-m_0|}(qb) S_{kljm}^{(m_0)}(b) \right|^2, \tag{15}$$

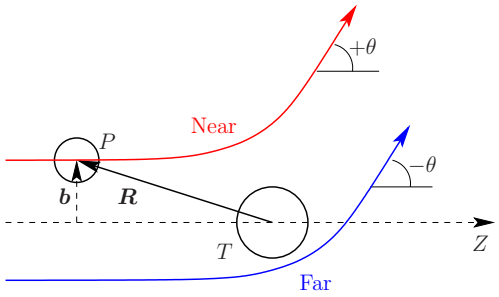

Figure 1. Schematic illustration of the Near and Far sides of the angular distribution.

where

$$S^{(m_0)}_{kljm}(\boldsymbol{b}) = \langle \phi_{kljm} | \widehat{\Psi}^{(m_0)}(\boldsymbol{b}, Z \to \infty) \rangle, \tag{16}$$

with ϕ_{kljm} the continuum wave function describing the broken up projectile in partial wave ljm.

To study the breakup process, we extend the N/F analysis to the angular distribution (15). As for the elastic scattering, the Bessel function is decomposed into the sum of two Hankel functions (12), which provide both N and F sides of the breakup cross section with the same interpretation, i.e. the contribution to breakup of the repulsive and attractive forces, respectively.

3. Elastic scattering

3.1. ^{11}Be *on* Pb *at* $69AMeV$

As a first step in our analysis, we study the elastic scattering of ^{11}Be on Pb at $69A$MeV. As mentioned earlier, ^{11}Be is the archetypical one-neutron halo nucleus. In our analysis, it is described as a ^{10}Be core in its 0^+ ground state to which one-neutron is loosely bound. We choose for the ^{10}Be-n interaction the potential developed in Ref. [20], which reproduces the $1/2^+$ ground state in the $1s1/2$ partial wave at 504 keV below the one-neutron separation threshold. This potential also reproduces the $1/2^-$ bound excited state in the $0p1/2$ orbital and the $5/2^+$ resonance in the $d5/2$ partial wave. We use the numerical parameters and the potentials V_{cT} and V_{fT} detailed in Ref. [14]. The numerical technique used to solve the DEA equation (7) is explained in Ref. [16]

The DEA elastic-scattering cross section is plotted in Fig. 2 as a ratio to Rutherford [21]. It presents a usual shape with a Coulomb rainbow at about 2° followed by an exponential drop. At larger angles, the angular distribution presents significant oscillations. The N/F decomposition shows that at forward angles the process is fully dominated by the N side, as expected for a (repulsive) Coulomb-dominated reaction [13]. Note that the forward-angles oscillations (i.e. below 2°) are observed in both the total cross section and its N side. The N/F interferences therefore cannot explain this feature of the angular distribution. At larger angles, i.e. around 8°, the N and F sides cross, explaining the oscillatory pattern of the total cross section. This shows in particular that attractive nuclear forces affect the elastic scattering mostly at large angles, as is expected from semiclassical models.

The whole interpretation of the N/F decomposition is based on the asymptotic behaviour of the Hankel functions (14). To validate this interpretation, we repeat the calculation of the cross section, its N and F sides using the asymptotics of the Bessel and Hankel functions. The angular distributions obtained in this way (dotted lines) are in excellent agreement with the exact ones, confirming our analysis of this N/F decomposition.

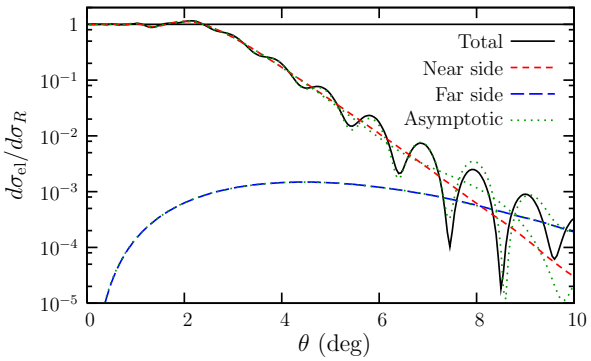

Figure 2. N/F analysis of the elastic scattering of ^{11}Be on Pb at 69AMeV [21].

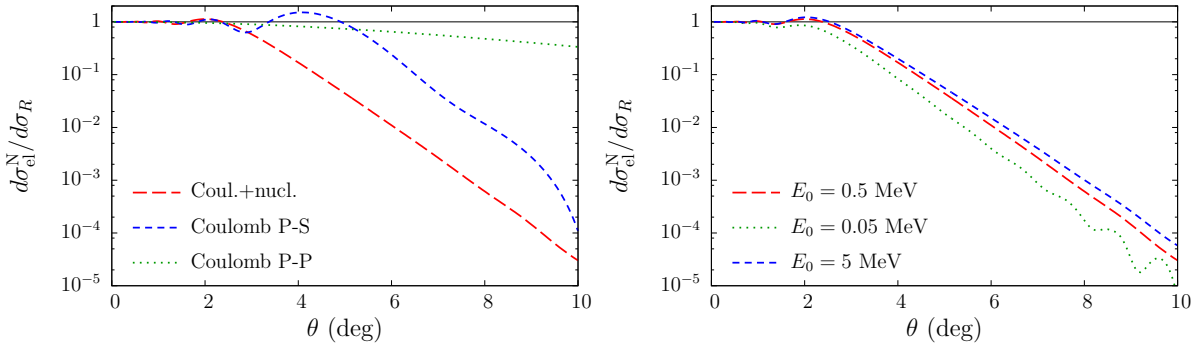

Figure 3. Sensitivity of the elastic-scattering cross section to the P-T interaction (left) and the extension of the halo (right).

3.2. Influence of P-T interaction

To better apprehend the influence of the choice of P-T interaction on the elastic scattering, we repeat the calculation with the sole Coulomb term of the nuclear optical potential (i.e. a point-sphere potential, P-S) and a purely point-point Coulomb interaction (P-P). The dominant N sides of the corresponding elastic-scattering cross sections are plotted in Fig. 3 (left). This change of potentials causes dramatic changes in the angular distribution. It mostly modifies the Coulomb rainbow. As the full optical potentials, the P-S interaction leads to a Coulomb rainbow, but its location is shifted from 2° to about 4°. On the contrary, no Coulomb rainbow is observed with the P-P interaction. This confirms that the features of the elastic-scattering cross section strongly depends on the choice of the optical potentials V_{cT} and V_{fT}.

Interestingly, the change in the elastic scattering cross section cannot be simply related to a transfer of flux towards the breakup channel, as postulated in Ref. [9]. Although the elastic scattering increases at large angles from the Coulomb + nuclear potential to the purely Coulomb interaction (first with P-S and then even more with P-P), the total breakup cross section increases as well, as shown in Table 1. Since the Coulomb rainbow appears only for the P-T potentials that account for the extension of the projectile and the target (i.e. the full optical potential or just its Coulomb component P-S), we now analyse the influence of the extension of the halo on these distributions.

Iteraction	P-P	P-S	C.+N.		
$\lvert E_0\rvert$ (MeV)	0.5	0.5	0.5	0.05	5
$\sigma_{\rm bu}$ (b)	2.58	2.10	1.70	23.57	0.07

Table 1. Total breakup cross sections corresponding to the calculations shown in Secs. 3.2 and 3.3 [21].

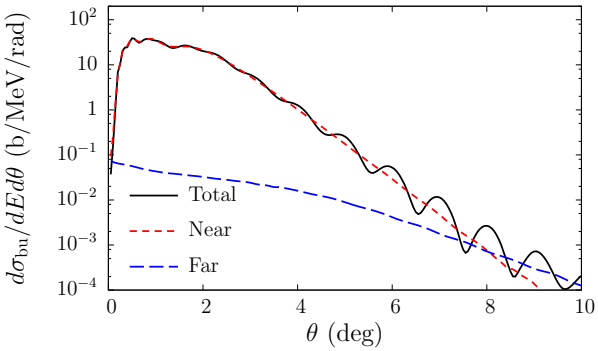

Figure 4. N/F decomposition of the breakup angular distribution for ^{11}Be on Pb at 69AMeV. The ^{10}Be-n relative energy is $E = 0.5$ MeV.

3.3. Influence of the size of the halo

To study the sensitivity of our results to the size of the halo, we repeat the DEA calculations adjusting the ^{10}Be-n potential to increase (reduce) the neutron separation energy $|E_0|$ of the ^{11}Be-like projectile in order to shrink (resp. expand) its halo. The N side of the elastic-scattering cross section is plotted as a ratio to Rutherford in Fig. 3 (right).

The slope of the exponential drop after the Coulomb rainbow is sensitive to E_0: Reducing the one-neutron separation energy of the projectile, i.e. expanding its halo, slightly reduces the elastic-scattering cross section. This effect could therefore be used to get information about the extension of the halo. However, this dependence remains small in comparison to the influence of the P-T potential [see Fig. 3 (left)]. There is thus little hope that observing the sole elastic-scattering cross section could provide unbiased information about the extension of the halo.

Since reducing $|E_0|$ increases the breakup cross section (see Table 1), we could believe that the transfer of flux to the breakup channel explains the change in the elastic-scattering cross section. However, since this increase is much more significant than the drop in the elastic-scattering cross section, our analysis confirms that there is no direct link between both effects, as suggested in Sec. 3.2.

4. Breakup of ^{11}Be on Pb at 69AMeV

To better comprehend the link between angular distributions for elastic scattering and breakup, we perform the same analysis as in Sec. 3 for the breakup cross section (15). For the breakup of ^{11}Be on Pb at 69AMeV, the angular distribution (solid line) and its N (short-dashed line) and F (long-dashed line) sides are plotted as a function of the scattering angle θ of the ^{10}Be-n centre of mass after dissociation [21] (see Fig. 4). The ^{10}Be-n relative energy is $E = 0.5$ MeV.

The features of the breakup angular distribution are very similar to those of the elastic-scattering cross section. First, the full calculation exhibits small oscillations at forward angles before an exponential drop starting at 2°, which is reminiscent of the Coulomb rainbow observed in the elastic-scattering cross section (see Fig. 2). Second, at forward angles, the breakup is dominated by its N side, just as in the elastic scattering. Finally, at larger angles, the total

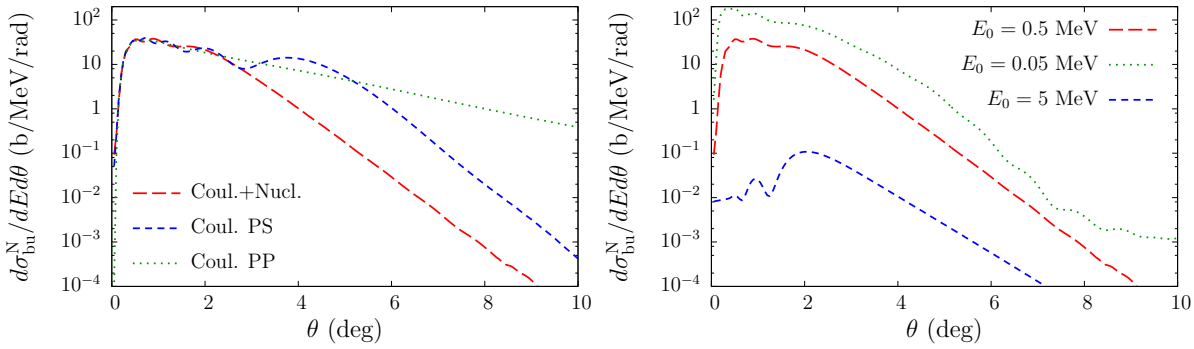

Figure 5. Sensitivity of the angular distribution for breakup to the P-T interaction (left) and the extension of the halo (right).

cross section exhibits oscillations that are explained by interferences between the N and F side, which cross at about 8°.

Fig. 5 shows the sensitivity of the breakup cross section to the P-T potential (left) and to the binding energy of the neutron $|E_0|$ (right). The similarity between elastic scattering and breakup is also observed here. Using the sole Coulomb part of the optical potentials (P-S) shifts the start of the exponential drop of the breakup cross section to 4°, as in the elastic-scattering one [see Fig. 3 (left)], and using the purely point-point Coulomb interaction (P-P) leads to no rainbow-like behaviour. Note that the larger breakup cross section obtained in the P-P case (see Table 1) is explained by this absence of Coulomb rainbow in the angular distribution for breakup. The sensitivity of breakup calculations to the neutron separation energy is also similar to that observed in the elastic channel. In particular for the slope of the drop after 2°, which becomes steeper when $|E_0|$ is reduced [see Fig. 3 (right)]. This confirms that there is no direct link between the drop observed in the elastic-scattering cross section and a possible loss of flux towards the breakup channel since both angular distributions vary in the same way when either the P-T interaction or the projectile structure are modified.

As shown in Ref. [22], these similarities can be semi-quantitatively explained within the Recoil Excitation and Breakup (REB) model developed by Johnson *et al* [23]. Within this adiabatic model, the angular distributions elegantly factorise into the product of an elastic-scattering cross section for a pointlike projectile and a form factor that accounts for the extension of the halo [23, 22]. The fact that the former appears in both factorisations and that it contains most of the angular dependence explains the similarity between the angular distributions. That analysis also suggests a new observable to study more precisely the halo structure. As observed in Fig. 3 (left) and Fig. 5 (left), the angular distributions are very sensitive to the choice of optical potentials. Since this sensitivity is very similar in both processes, taking the ratio of two angular distributions removes most of the dependence on the choice of the P-T potentials. Such a ratio emphasises the nuclear-structure content of the angular distributions [22].

5. Conclusion and prospect

In this work, we analyse theoretically elastic-scattering and breakup reactions of halo nuclei through a N/F decomposition of their angular distributions [21]. The calculations are performed for ^{11}Be, the archetypical one-neutron halo nucleus, impinging on Pb at 69AMeV, which corresponds to the experimental conditions of Ref. [10]. The calculations are performed with the DEA, a reliable and accurate reaction model in which elastic scatering and breakup are described simultaneously [11, 14].

Our analysis shows that at intermediate energy, the angular distribution for breakup is very

similar to the elastic-scattering cross section: Both present a Coulomb rainbow at the same scattering angle θ, they are both N-side dominated at forward angles, they both exhibit similar sensitivity to the choice of P-T interaction and to the binding energy of the halo neutron. These results suggest that the projectile is scattered by the target in a similar way whether it remains bound or it is broken up. This can be semi-quantitatively understood within the REB model [22, 23].

The present analysis also suggests that there is no obvious link between the drop observed in the elastic-scattering cross section and a possible transfer of probability flux towards the breakup channel, as postulated in Ref. [9]. Since the work of Di Pietro *et al* has been performed at lower energy (around the Coulomb barrier), our conclusions cannot be directly transposed to their study. A similar analysis within the CDCC framework [24] is planned to see how elastic scattering and breakup are related to each other at low energy. Moreover, recent progresses having been made in the modelling of reactions involving two-neutron halo nuclei [25, 26], an extension of this work for Borromean systems is also planned.

Acknowledgement
M. H. is supported by the Brazilian agencies CNPq and FAPESP. This text presents research results of the Belgian Research Initiative on eXotic nuclei (BriX), programme P6/23 on interuniversity attraction poles of the Belgian Federal Science Policy Office.

References

[1] I. Tanihata *et al.*, Phys. Lett. **B160**, 380 (1985).
[2] I. Tanihata *et al.*, Phys. Rev. Lett. **55**, 2676 (1985).
[3] P. G. Hansen and B. Jonson, Europhys. Lett. **4**, 409 (1987).
[4] I. Tanihata, J. Phys. G **22**, 157 (1996).
[5] B. Jonson, Phys. Rep. **389**, 1 (2004).
[6] J. Al-Khalili and F. M. Nunes, J. Phys. G **29**, R89 (2003).
[7] G. Baur, K. Hencken and D. Trautmann, Prog. Part. Nucl. Phys. **51**, 487 (2003).
[8] T. Matsumoto, T. Egami, K. Ogata, Y. Iseri, M. Kamimura and M. Yahiro, Phys. Rev. C **73**, 051602(R) (2006).
[9] A. Di Pietro *et al.*, Phys. Rev. Lett. **105**, 022701 (2010).
[10] N. Fukuda *et al.*, Phys. Rev. C **70**, 054606 (2004).
[11] D. Baye, P. Capel and G. Goldstein, Phys. Rev. Lett. **95**, 082502 (2005).
[12] B. V. Carlson, M. P. I. Filho and M. S. Hussein, Phys. Lett. **B154**, 89 (1985).
[13] M. S. Hussein and K. W. McVoy, Prog. Part. Nucl. Phys. **12**, 103 (1984).
[14] G. Goldstein, D. Baye and P. Capel, Phys. Rev. C **73**, 024602 (2006).
[15] D. Baye and P. Capel *Breakup Reaction Models for Two and Three-Cluster Projectiles*, in *Cluster in Nuclei, Vol. 2*, edited by C. Beck, Lecture Notes in Physics **848** (Springer-Verlag, Heidelberg, 2012) p. 121.
[16] P. Capel, D. Baye and V. S. Melezhik, Phys. Rev. C **68**, 014612 (2003).
[17] G. Goldstein, P. Capel and D. Baye, Phys. Rev. C **76**, 024608 (2007).
[18] P. Capel, H. Esbensen and F. M. Nunes, Phys. Rev. C **85**, 044604 (2012).
[19] M. Abramowitz and I. A. Stegun, *Handbook of Mathematical Functions* (Dover, New York, 1970).
[20] P. Capel, G. Goldstein and D. Baye, Phys. Rev. C **70**, 054606 (2004).
[21] P. Capel, M. S. Hussein and D. Baye, Phys. Lett. **B693**, 448 (2010).
[22] P. Capel, R. C. Johnson and F. M. Nunes, Phys. Lett. **B705**, 112 (2011).
[23] R. C. Johnson, J. S. Al-Khalili and J. A. Tostevin, Phys. Rev. Lett. **79**, 2771 (1997).
[24] T. Druet, D. Baye, P. Descouvemont and J.-M. Sparenberg, Nucl. Phys. **A845**, 88 (2010).
[25] D. Baye, P. Capel, P. Descouvemont and Y. Suzuki, Phys. Rev. C **79**, 024607 (2009).
[26] E. C. Pinilla, P. Descouvemont and D. Baye, Phys. Rev. C **85**, 054610 (2012).